Chapter V
Ocean response to sub-seasonal wind forcing

V.1 Introduction:

In this chapter, I use an OGCM to explore dynamical aspects of the ocean response to sub-seasonal surface wind variability. I examine the response of the central and eastern equatorial Pacific to the Type C WWE and to composite MJO forcing. I use these analyses to understand the dynamical connections which are the source of the statistical associations between SST variability and sub-seasonal wind variability.

In the previous chapters I described the typical surface wind structures associated with WWEs (Chapter II) and with the MJO (Chapter IV). I argued that WWEs and the MJO were distinct modes of variability (Chapter IV); and examined statistical relationships of the MJO and WWEs to El Niño. Equatorial WWEs are associated with warming at the onset of El Niño and warm anomaly maintenance during El Niño (Chapter III); there is no correlation between the MJO and El Niño indicators (Slingo *et al.* 1999, Hendon *et al*. 2000, Harrison and Vecchi 2000, Vecchi and Harrison 2000.b, Chapter IV).

I here attempt to reproduce the statistical associations of the MJO and WWEs to eastern Pacific SSTA, using an OGCM; I also examine the mechanisms responsible for those changes. I find that the composite MJO zonal stress anomalies do not drive central/ eastern equatorial Pacific waveguide warming in the model; the composite MJO does not provide a mechanism for waveguide warming during the onset of El Niño. I find that equatorial WWEs force eastern and central equatorial Pacific SSTA changes which resemble those observed in the composite (see Chapter III); WWEs are a mechanism for the onset of El Niño. I find that superimposing a composite Type C WWE on a composite MJO leads to eastern Pacific SST warming of a similar structure to that following the WWE.

Analyses of OGCM response to idealized WWE zonal wind anomalies have found

that WWE-driven circulation changes produce SST warming in the eastern and central Pacific equatorial waveguide (Harrison and Giese 1988, Giese and Harrison 1990, 1991), with SST changes as large as 0.5°C from a single WWE. Those experiments were performed using idealized WWEs with realistic meridional and time-scales, but the zonal scale was hypothetical; the experiments described in this chapter are done with realistic (x,y,t) scales.

Harrison and Giese (1988) found that while changes in the zonal surface current field tended to coincide with the first baroclinic Kelvin pulse, the SST changes in the eastern equatorial Pacific were dominated by the second baroclinic mode. An unexpected finding of Harrison and Giese (1988) was that anomalous meridional advection of heat has a dominant term in the eastern Pacific SST warming. It was suggested that modulation of the tropical instability wave (TIW) field by the WWE driven Kelvin pulses was a mechanism for the anomalous meridional advection.

It has been suggested that intra-seasonal surface wind variability in the western and central Pacific, driven by the MJO, may be important to the onset of waveguide SST warming during El Niño (Lau and Chan 1986, 1988, Lau and Shen 1988, Weickman 1991, Kessler *et al.* 1995, Moore and Kleeman 1999). Analysis of the potential role of the MJO on tropical Pacific SST have idealized the MJO surface wind variability as a sinusoid confined to the western equatorial Pacific (Kessler *et al.* 1995, Kessler and Kleeman 2000). In the previous Chapter, I argued that the surface wind variability associated with the MJO does not much resemble those idealized models; the near-equatorial surface wind anomalies extend across much of the central and eastern Pacific (see Section IV.3.a). In a recent description of the abrupt termination of the 1997-98 El Niño event, Takayabu *et al.* (1999) argue that easterly stresses driven by the MJO were responsible for the return to normal SST. I explore the potential role of the composite MJO in El Niño using the composite zonal stress anomaly fields and the OGCM.

In the following sections I describe the modeling work done to explore the role of

sub-seasonal variability in El Niño. Section 2 describes the model and the different experiments run. Section 3 discusses the results for the MJO experiments. Section 4 shows the results for the MJO experiment. Finally, Section 5 gives a summary and conclusions.

2. Data and Methods:

To explore to oceanic response to the composite zonal wind stress pattern, I use the NOAA primitive equation OGCM, which has been used in many studies of the tropical Pacific (Philander and Seigel 1985, Harrison and Giese 1988, Philander *et al.* 1987, Philander *et al*. 1989, Giese and Harrison 1991) and is the basis of NOAA's operational tropical Pacific Ocean analysis program (Ji *et al.* 1995). The model grid is an Arakawa-B grid, which spans the tropical Pacific from 130°E to 90°W (by 1° longitude) and 30°S to 50°N (by 1/3° from 10°S to 10°N, stretching to 2.3° at 30°S and 2.9° at 50°N); there are 27 levels in the vertical, with 10 m resolution in the upper 100 meters and stretching to 650m at 3800m depth. The model timestep is 3600 seconds (1 hour). The model topography includes realistic coastlines, but no bottom topography. Vertical mixing is parametrized using the Richardson number dependent scheme of Pacanowski and Philander (1981), with the background wind mixing parameter set at 10 cm^2s^{-1}, the maximum friction coefficient at 50 cm^2s^{-1}, the background mixing and diffusion are set at 1.0 cm^2s^{-1} and 0.1 cm^2s^{-1}, respectively. Horizontal mixing is parametrized as eddy diffusion, with momentum mixed using A_m of $1.0 \infty 10^7$ cm^2s^{-1}, and heat diffused using A_h of $2.0 \infty 10^7$ cm^2s^{-1}.

The model is spun up for five years using the annual mean climatological wind stress field of Harrison (1989), a sixth year is run as the control experiment. Surface heat flux is parametrized as in Harrison (1989), using the annual mean air temperature from the COADS climatology (Woodruff *et al.* 1987). Sea surface salinity is restored to the annual mean Levitus climatology using a 50 day restoring timescale. Figure V.1 shows the SST and wind-stress fields for the spin-up run, along with the annual mean SST from COADS.

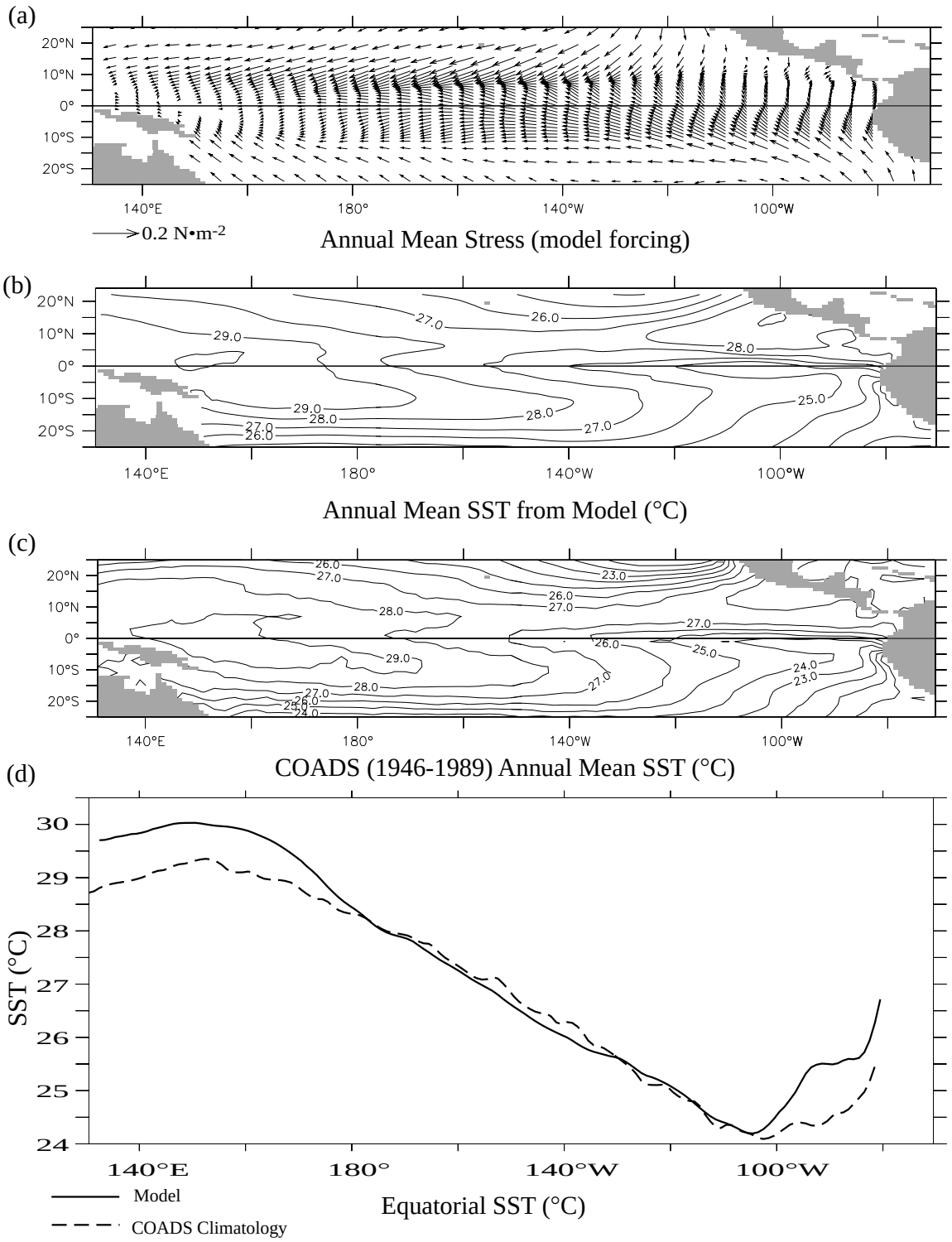

Figure V.1: (a) Annual mean surface wind stress used to initialize the model. (b) Annual mean SST from the OGCM. (c) Annual mean climatological SST. (d) Line plot of model and climatological SST along equatorial Pacific.

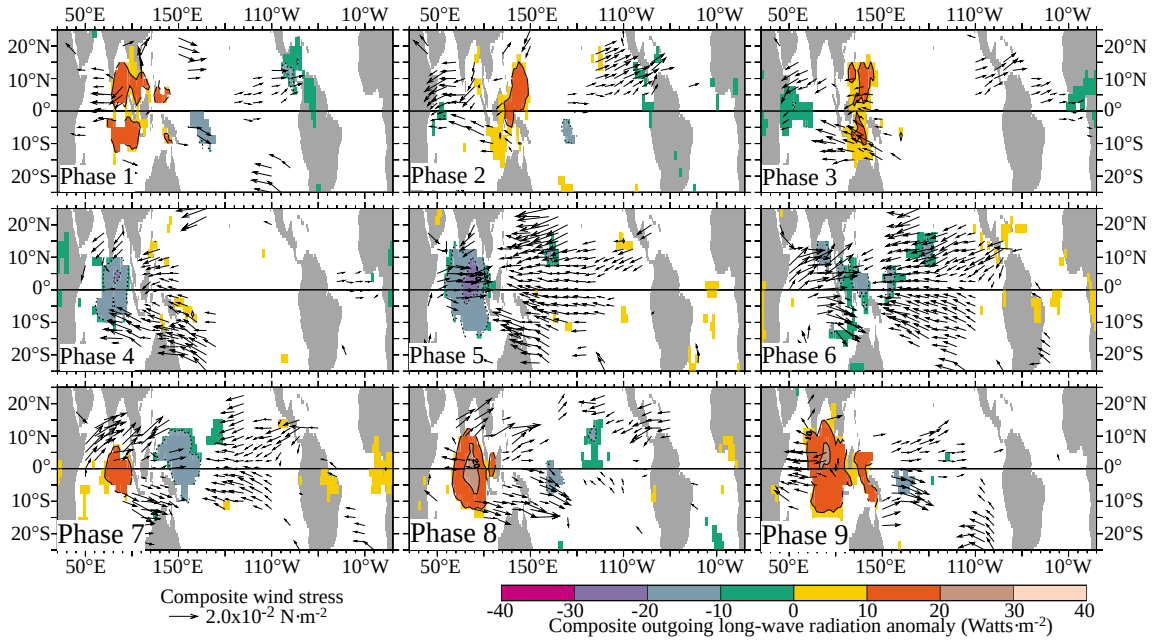

Figure V.2: All-event MJO composite surface wind stress and OLR anomalies for each of the 9 Phases defined by Maloney and Hartman (1998). Vectors show the compositestress values for which eitther the zonal or meridional component is significant at the 99% level. Shading indicates values of OLRA significant at the 99% confidence level.

Notice that the near equatorial SST in the central Pacific between 180° and 110°W is well reproduced by the model; while the negative zonal SST gradient between 160°E and 180° and the positive zonal SST gradient between 100°W and the coast are both too large in the model (Figure V.1.d). However, the SST gradients and current fields across most of the central and eastern Pacific, giving a realistic enough background state for these experiments.

The MJO experiments are forced by adding the 99% statistically significant all-event composite zonal stress anomaly field to the climatological stress field. The composite is evaluated as in Chapter IV, using the MJO list as defined using the Maloney and Hartmann (1998) MJO index, and the European Centre for Medium Range Weather Forecasts (ECMWF) 2.5°∞2.5° gridded 12-hourly operational surface wind-stress analysis from 1986-1998 (ECMWF 1989). Anomalies were computed from a monthly climatology, 1986-1996. Figure V.2 shows a vector map of the 99% significant surface wind-stress fields associated with the MJO, and Figure V.3 shows a shaded plot of the evolution of the 99% significant

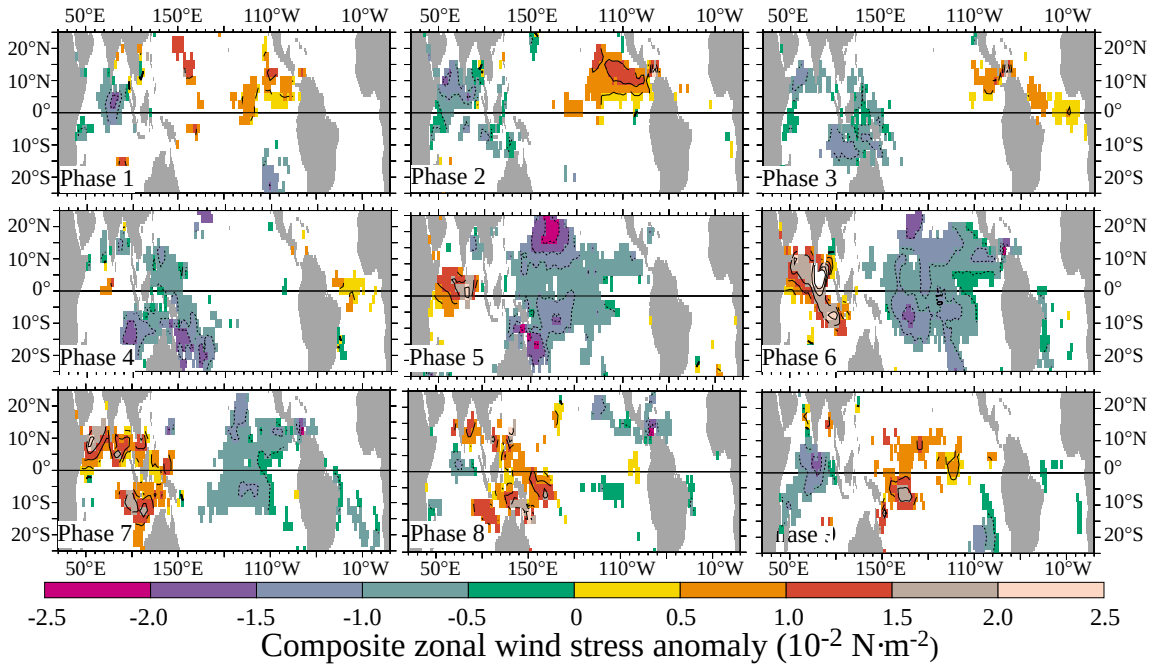

Figure V.3: Shaded plots of the evolution of the 99% significant all-event MJO composite zonal stress anomaly field. Only values for which the zonal stress anomaly is significantly different from zero at the 99% confidence level are shown.

zonal stress fields. Notice how, as in the MJO surface wind fields, the composite is dominated by easterly stress anomalies over the eastern and central Pacific. Through the lifetime of an MJO event, the western Pacific stress anomalies exhibit periods of both easterly and westerly stress.

Five MJO forcing experiments were performed (M1-M5), and are summarized in Table V.1; three examine the effect of a single MJO period on the tropical Pacific, and the fourth examines the effect of four sequential MJOs. The fifth experiment removes the mean

Table V.1: List of MJO experiments used in this Chapter.

Experiment #	*Anomalous surface zonal stress forcing used*
M1	*1 Period of 99% significant composite zonal stress anomaly.*
M2	*1 Period of 99% significant composite zonal stress anomaly west of 165°E, zero east of 165°E.*
M3	*1 Period of 99% significant composite zonal stress anomaly east of 165°E, zero west of 165°E.*
M4	*4 Periods of 99% significant composite zonal stress anomaly.*
M5	*4 Periods of 99% signficant composite zonal stress anomaly, with the mean over one MJO period removed.*

stresses associated with the MJO and examines the ocean response. For the experiments shown here each MJO Phase was taken to be 5 days long (using Phase lengths 7 and 10 days, or using 3 consecutive MJOs, did not affect the main results). To minimize transients, I begin each MJO on Phase 3 and run through Phase 2 - the Phases with smallest equatorial Pacific zonal stress associations (see Figure V.2 and V.3; starting the MJO on Phase 1 does not alter the main results).

To examine the response to the OGCM to Type C WWEs, I run a series of experiments using the Gaussian zonal stress anomaly model, with the scales described in Chapter II. The zonal *e*-folding scale is 18°, the meridional *e*-folding scale is 5° and the temporal *e*-folding scale is 3.5 days (see Table II.3). The composite Type C WWE stress has an amplitude near 0.06 $N \cdot m^{-2}$, I use three different amplitude WWEs to test the amplitude dependence of the solutions: 0.06 $N \cdot m^{-2}$, 0.1 $N \cdot m^{-2}$ and 0.2 $N \cdot m^{-2s}$. Table V.2 summarizes the experiments run. Experiments C1 through C3 examine the effect of a single Type C WWE on the annual mean ocean; Experiments C4 through C6 examine the effect of multiple WWEs. Experiment CM explores the response of the Tropical Pacific to a Type C WWE superimposed on a composite MJO.

Table V.2: List of the Type C WWE experiments discussed in this Chapter.

Experiment #	*Anomalous surface zonal stress forcing used*
C1	*One Gaussian Type C WWE (0.06 $N \cdot m^{-2}$), centered on Jan-15.*
C2	*One Gaussian Type C WWE (0.1 $N \cdot m^{-2}$), centered on Jan-15.*
C3	*One Gaussian Type C WWE (0.2 $N \cdot m^{-2}$), centered on Jan-15.*
C4	*Three Gaussian Type C WWEs (0.06 $N \cdot m^{-2}$), centered on Jan-15, Feb-4, and Feb-24.*
C5	*Three Gaussian Type C WWEs (0.1 $N \cdot m^{-2}$), centered on Jan-15, Feb-4, and Feb 24.*
C6	*Three Gaussian Type C WWEs (0.2 $N \cdot m^{-2}$), centered on Jan-15, Feb-4 and Feb-24.*
C7	*Type C WWEs (0.1 $N \cdot m^{-2}$), every 20 days starting on Jan-15 and continuing through run.*
CM	*One Composite MJO + 1 Type C (0.06 $N \cdot m^{-2}$) WWE centered on Phase 6 of the MJO.*

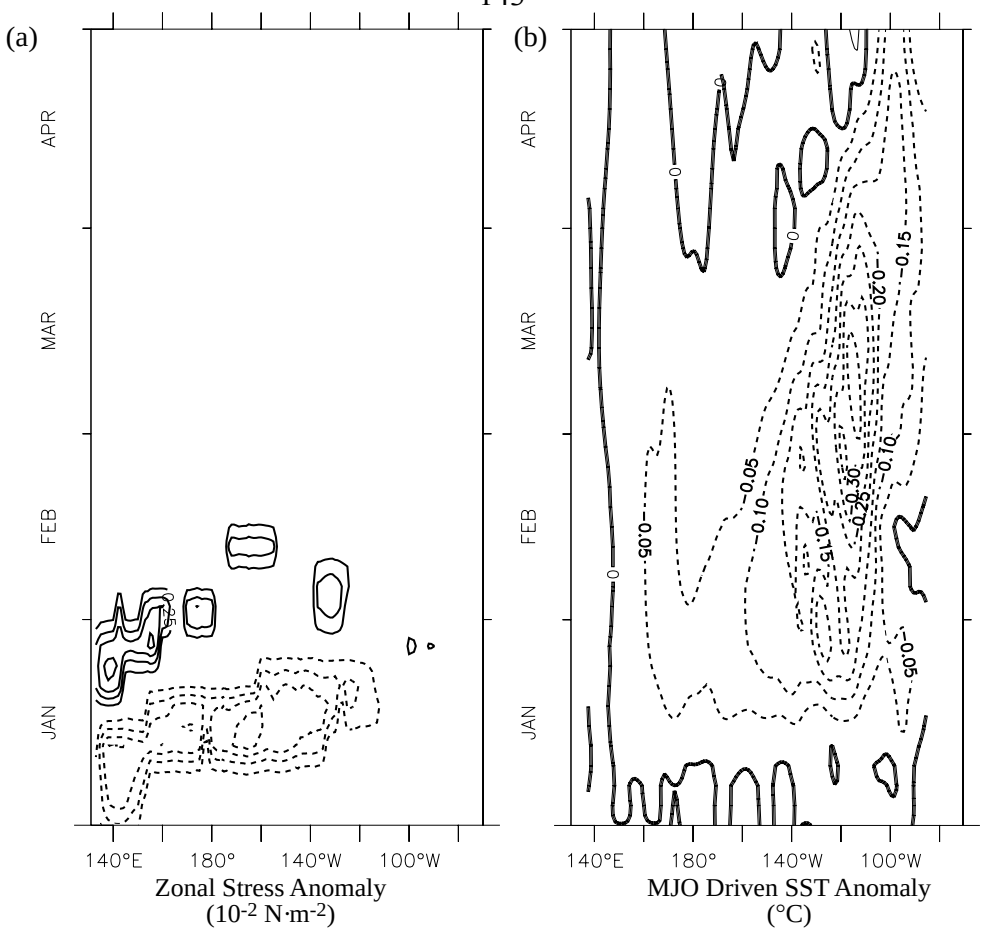

Figure V.4: (a) Zonal stress anomaly at the equator from Experiment M1. Contour interval is $0.25 \infty 10^{-2}$ N·m^{-2}. (b) MJO-driven SSTA along the equator, from Experiment M1. Notice how the composite MJO drives central and eastern Pacific surface cooling during and following the wind anomalies. SSTA is zonally smoothed with an 11° cosine filter in longitude to remove TIWs. Contour interval is 0.05°C.

3. Ocean Response to the MJO:

Because easterly stress anomalies are very effective at cooling local SST by horizontal and vertical advection, and because the MJO-related easterly stress anomalies exceed the westerly stress anomalies in space and intensity, one should expect the MJO composite zonal wind-stress anomaly to cool the equatorial Pacific. The OGCM results confirm that expectation. The response of the equatorial Pacific SSTA to a single period of composite MJO zonal stress anomaly (Experiment M1) is shown in Figure V.4. As expected from the composite zonal stress fields, the surface of the eastern and central Pacific weakly cools

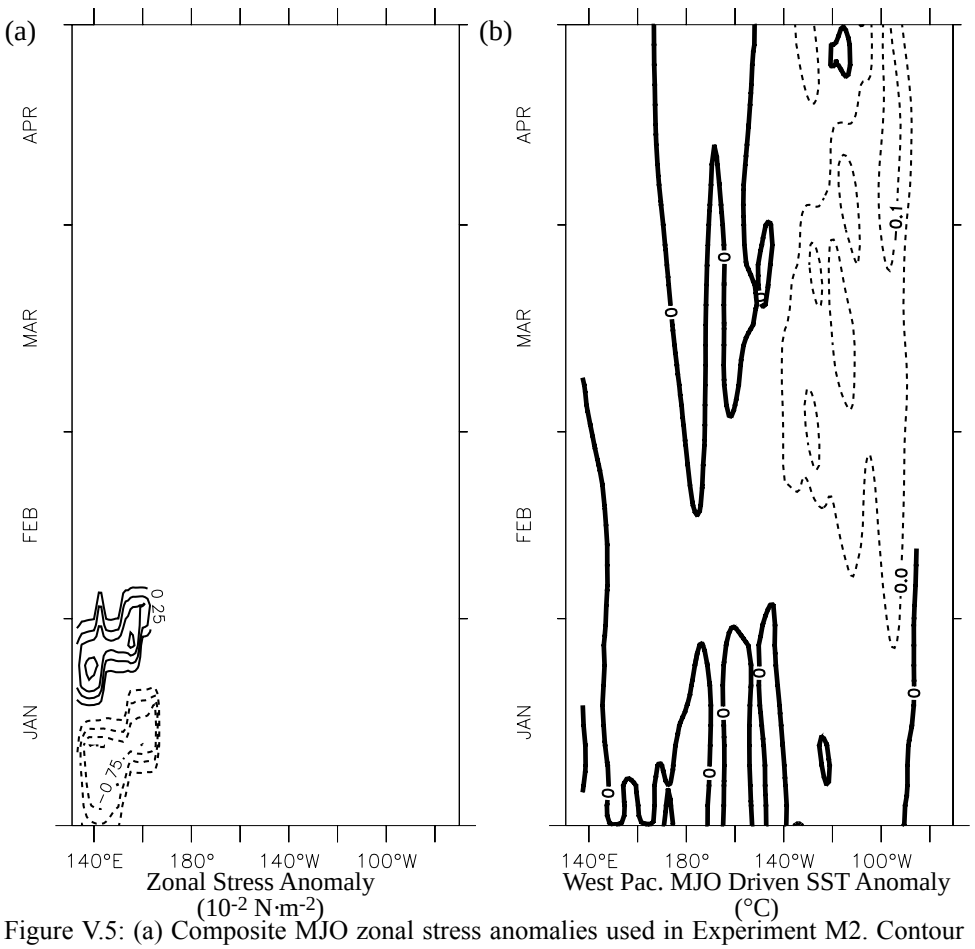

Figure V.5: (a) Composite MJO zonal stress anomalies used in Experiment M2. Contour interval is $0.25 \infty 10^{-2}$ N·m^{-2}. (b) SSTA deiven by the western Pacific part of the MJO zonal wind stress forcing (Experiment M2). SSTA is zonally smoothed with an 11° cosine filter in longitude to remove TIWs. Contour interval is 0.05°C.

during the lifetime of the MJO. There is also weak warming following the event, which does not exceed 0.1°C. The cooling occurs during the MJO Phases with easterly stress anomalies over the eastern and central Pacific (Phases 5-7) under the stress anomalies. The cooling enhances in the eastern Pacific (between 140°W and 100°W) in the month that follows the anomalous forcing, and then begins to disappear.

To parse the effects of the near-sinusoidal western Pacific stress anomaly fields, and the easterly stress surge in the central and eastern Pacific, I ran experiments M2 and M3. Experiment M2 is run with only the western Pacific zonal stress anomaly field (west of 170°E), while M3 is run with only the eastern Pacific zonal stress anomaly field (east of 170°W). The SST changes driven by the western Pacific part of the MJO anomalies are

shown in Figure V.5, and Figure V.6 shows the response to the central and eastern Pacific part of the MJO. The response to the entire MJO forcing resembles a superposition of the response to the western Pacific forcing and the eastern Pacific forcing, since the magnitude of the stress anomalies is small, the linear character of the response is not unexpected.

The western Pacific part of the MJO zonal stress anomaly forcing drives weak eastern Pacific SST cooling (Figure V.5). The cooling in the far eastern Pacific is weak (less than 0.1°C) and begins about 30 days after the beginning of the anomalous zonal stress in the western Pacific. The SSTA cooling driven by the western Pacific zonal stress anomalies accounts for approximately one third the far eastern Pacific cooling; the western Pacific zonal stress anomalies have little effect on the central Pacific SST. It must be noted that the zonal SST gradients in the region of largest west-Pacific-MJO SST response (the far-eastern Pacific) are overestimated in the background state when compared with COADS climatology (see Figure V.1). The response of the model ocean to the western Pacific part of the MJO is likely overestimated due to this.

The equatorial SSTA driven by the central and eastern Pacific part of the MJO zonal stress anomaly field is dominated by cooling through the event (Figure V.6). There is very little western Pacific SSTA associated with the stress anomalies from Experiment M3, the main changes occur underneath and to the east of the easterly surge. The cooling begins across the central and eastern part of the basin upon the arrival of the easterly stress anomalies, A front develops and moves east over the months following the forcing, with cooled SST to the east of it, and normal SST to the west of it. The front reaches the far eastern Pacific by mid-April, about two and a half months after the end of the easterly anomalies. The central and eastern Pacific part of the MJO forcing is responsible for practically all the cooling in the central part of the basin (between 165°E and 140°W), and about two thirds of the surface cooling east of 140°W.

Because the effect of one MJO event is to cool the eastern Pacific SST with weak

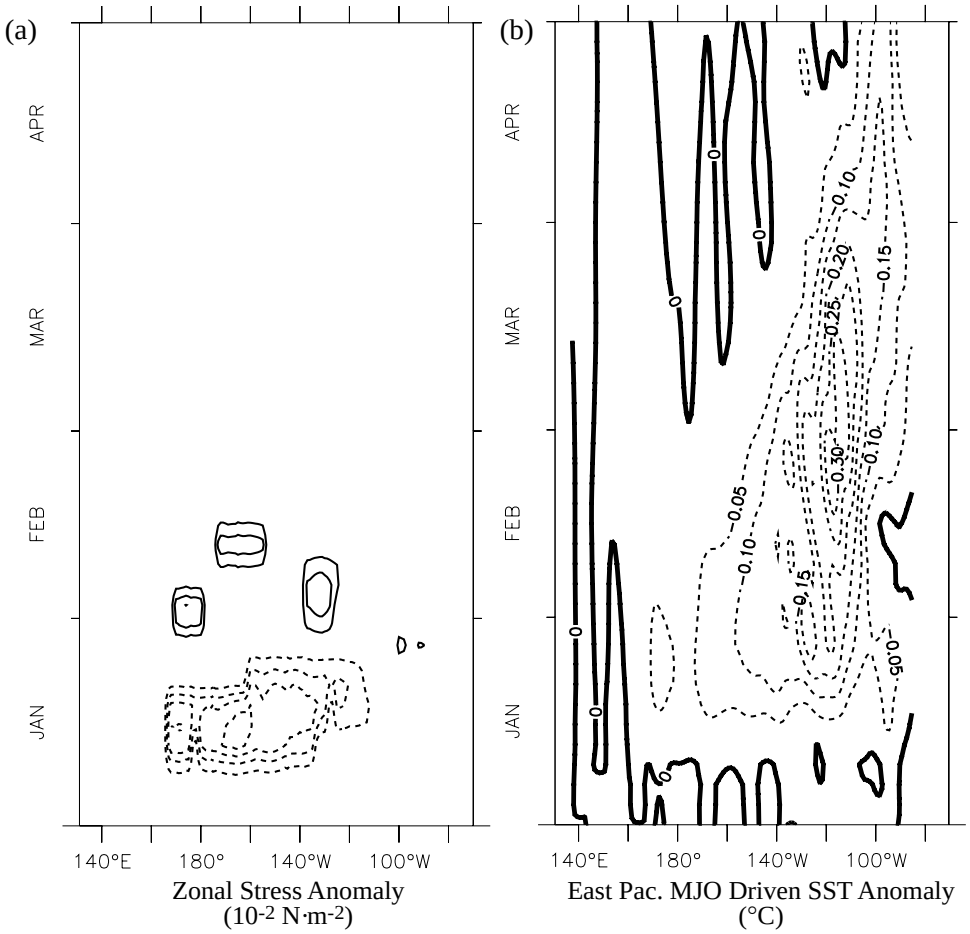

Figure V.6: (a) zonal stress anomalies used in Exp M3. Contour interval is $0.25 \infty 10^{-2}$ N·m^{-2}. (b) SSTA deiven by the central and eastern Pacific part of the MJO zonal wind stress forcing (Experiment M3). SSTA is zonally smoothed with an 11° cosine filter in longitude to remove TIWs. Contour interval is 0.05°C.

warming following the event, I expect a sequence of MJO events to lead to cooling of the eastern equatorial Pacific. The OGCM confirms this expectation, Figure V.7 shows the SSTA result of forcing with four consecutive cycles of the MJO composite zonal wind stress anomalies (smoothed in longitude with an 11° cosine filter to remove tropical instability waves). Cooling prevails over the central and eastern equatorial Pacific during the period in which MJO forcing was imposed. Subsequent to the MJO forcing interval very weak central or eastern Pacific warming occurs which does not extend across any large band of the Pacific. Rather than warm the eastern equatorial Pacific, as has been suggested recently, the effect of a sequence of composite MJO events is to weakly cool the surface of

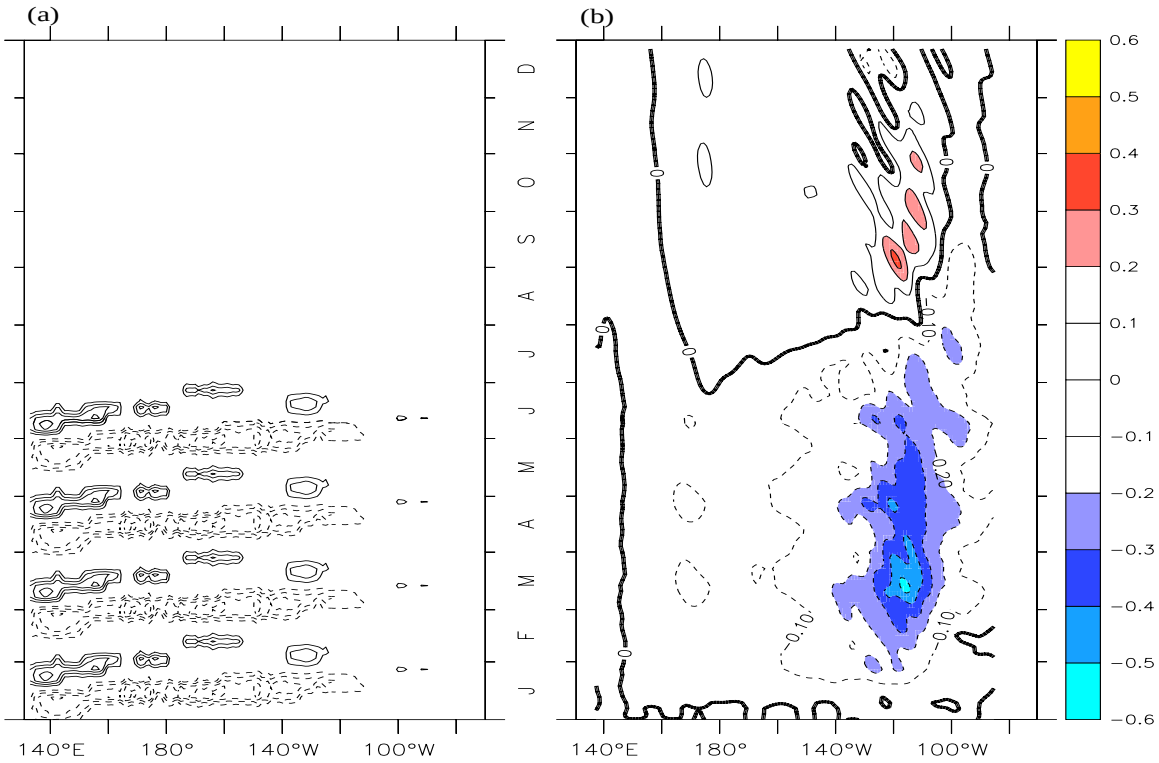

Figure V.7: (a) Four periods of composite MJO surface zonal stress anomaly forcing (Experiment M4). Contour interval is $0.25 \infty 10^{-2}$ N·m^{-2}. (b) SSTA response to the four periods of composite MJO surface zonal stress anomaly forcing. SSTA is zonally smoothed with an 11° cosine filter in longitude to remove TIWs.

the eastern equatorial Pacific.

The mean equatorial easterlies in the central and eastern Pacific, which appear in the MJO composite are possibly an artifact of the MJO compositing technique or the climatoloy used. It is important to consider the effect of the MJO composite zonal stress fields which do not have a net momentum flux into the eastern and central equatorial Pacific. Experiment M5 examines the effect of driving the OGCM with four cycles of the MJO composite zonal stress, with its mean subtracted. Figure V.8 shows the SSTA and the zonal stress anomalies from experiment M5. These should be contrasted with those shown in Figure V.7. Notice how the SSTA changes in the eastern and central Pacific in the presence of the MJO anomalies is still not for warming; there is very weak cooling in the eastern and central equatorial Pacific. Following the MJO forcing there is some weak warming in the central Pacific. This warming is localized, and is associated with the termination of the

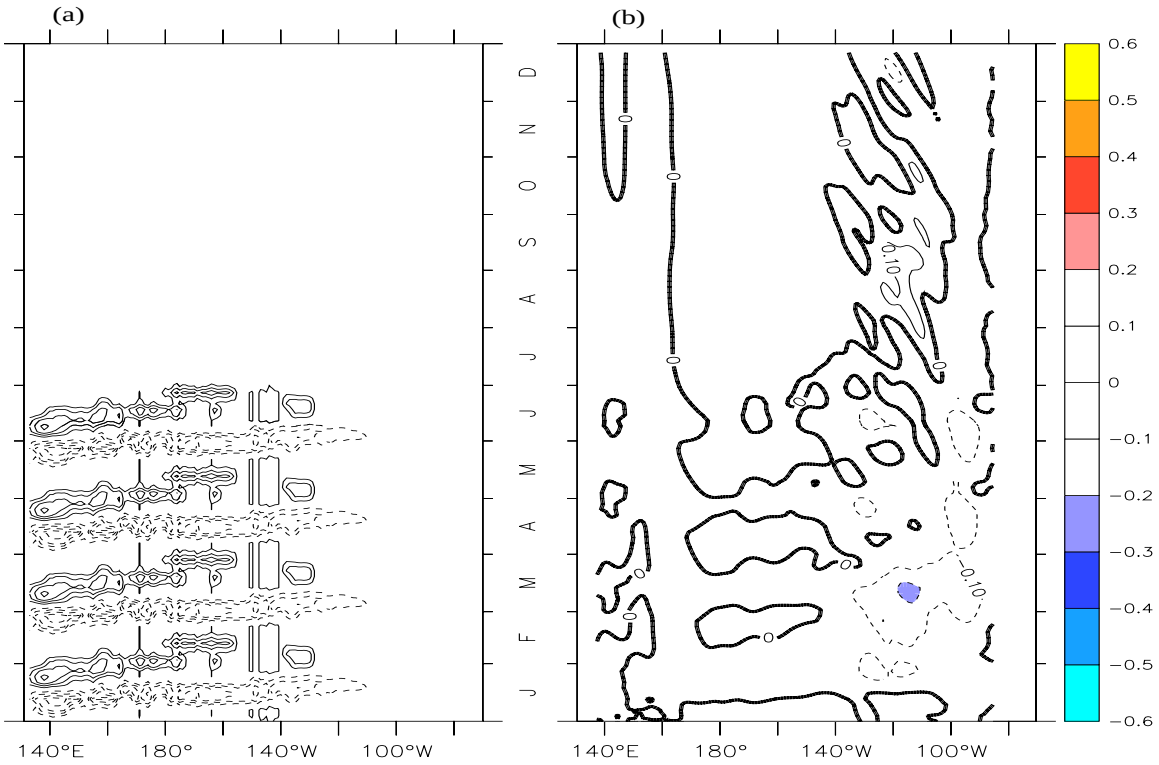

Figure V.8: (a) Four periods of composite MJO surface zonal stress anomaly forcing with the mean over an MJO removed (Experiment M5). Contour interval is $0.25 \infty 10^{-2}$ N·m^{-2}. (b) SSTA response to the four periods of composite MJO surface zonal stress anomaly forcing. SSTA is zonally smoothed with an 11° cosine filter in longitude to remove TIWs.

MJO forcing. Even with the mean eastern and central equatorial Pacific easterlies removed, the composite MJO suraface zonal stress anomalies do not drive warming in the model.

Figure V.9 shows the thermocline anomalies, approximated as the depth of the 20°C isotherm, driven by the four period composite MJO zonal stress anomalies (Experiment M4). Notice how during the period of anomalous forcing (January through June) the western and central Pacific thermocline anomaly evolution is dominated by a series of eastward propagating pulses of alternating shoaling and deepening. Meanwhile, the eastern Pacific thermocline is dominated by a shoaling through the forcing period, with slight variability at the period of the MJO. West of 140°W, the SSTA changes driven by the MJO are not a direct representation of the MJO driven thermocline changes; while the MJO driven thermocline changes are primarily oscillatory, the SSTA is dominated by cooling with a superimposed oscillation. In the eastern Pacific, the SSTA and thermocline depth anomaly patterns corre-

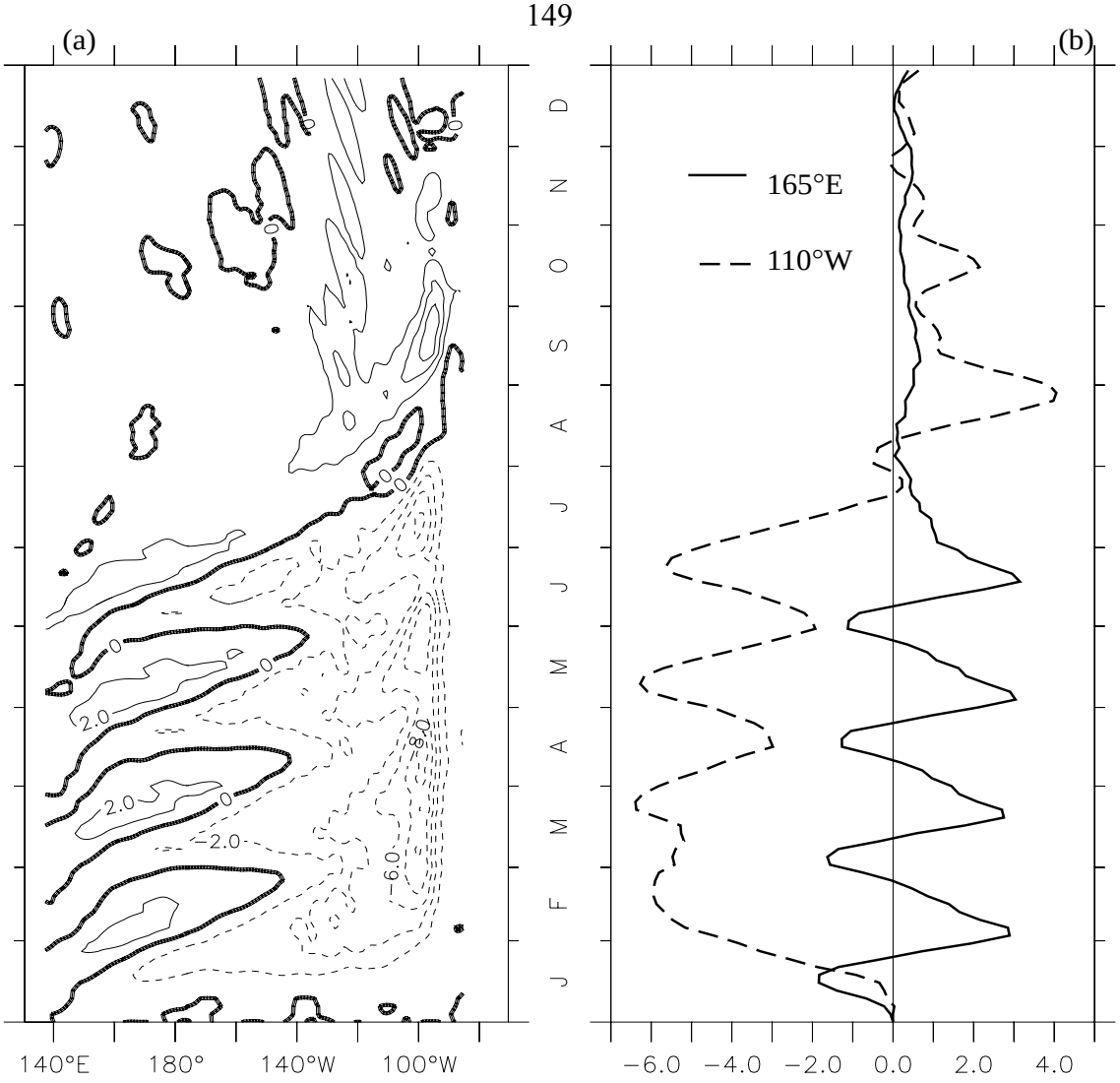

Figure V.9: (a) Time-longitude contour plot of the 15° cosine smoothed (in longitude - to remove TIWs) equatorial thermocline depth anomaly driven by four consecutive MJOs (Experiment M4). Contour interval is 2 meters. (b) Time-series of the 15° cosine smoothed thermocline depth anomalies at (165°E,0°) and (110°W,0°).

spond more closely. Following the final MJO event in the series there is a pulse of thermocline deepening which propagates east across the basin. These relationships between SSTA and thermocline depth anomalies are consistent with the long-term SSTA/thermocline depth anomaly correlations, which show that only in the eastern Pacific there are statistically significant correlations between SSTA and thermocline depth anomaly (see Harrison and Vecchi 2000). The arrival of the pulse of downwelling corresponds with the return of SST to normal in the eastern Pacific.

4. Ocean Response to Type C WWEs:

I now examine the response of the OGCM to the Type C WWE forcing experiments. First I attempt to reproduce the SSTA changes which appear in the Type C WWE composite (see Section III.3). I then examine the mechanisms responsible for the SSTA changes in the model.

a. Comparison to Data:

The composite SSTA changes following Type C WWEs were dominated by warming of the eastern and central equatorial Pacific, and by weak cooling along the western edge of the WWE (see Chapter III). The OGCM forced with the idealized (using realistic scales) zonal stress anomaly fields for the Type C WWE reproduce many of the characteristics of the composite SSTA change fields. Figure V.10 shows the composite SSTA change 60 days after the WWE center date for Experiments C1,C2 and C3, and from the Case REGULAR Type C composite. Model data are smoothed with a 30-day boxcar filter to remove TIWs.

The structure of the model SST changes agree with the composite structures in the region 160°W to 100°W, with the amplitude being best reproduced by Experiment C3. The model warming in the central Pacific is concentrated east of 160°W, as in the composite. The model gives weak warming in the far eastern Pacific and along the coast of South America, consistent with the compositing results.

The main qualitative differences are west of the Dateline and east of 100°W, where the initial model SST gradients were larger than climatology. The model zonal SST gradient between 160°E and the Dateline is about twice climatology; if the anomalous zonal advection term in that area is halved (after the model is run) and the temperature tendency is recomputed, there is no equatorial warming west of the Dateline. Similarly, if the zonal SST gradient east of 100°W is artificially reduced after the model is run, the warming in the far-

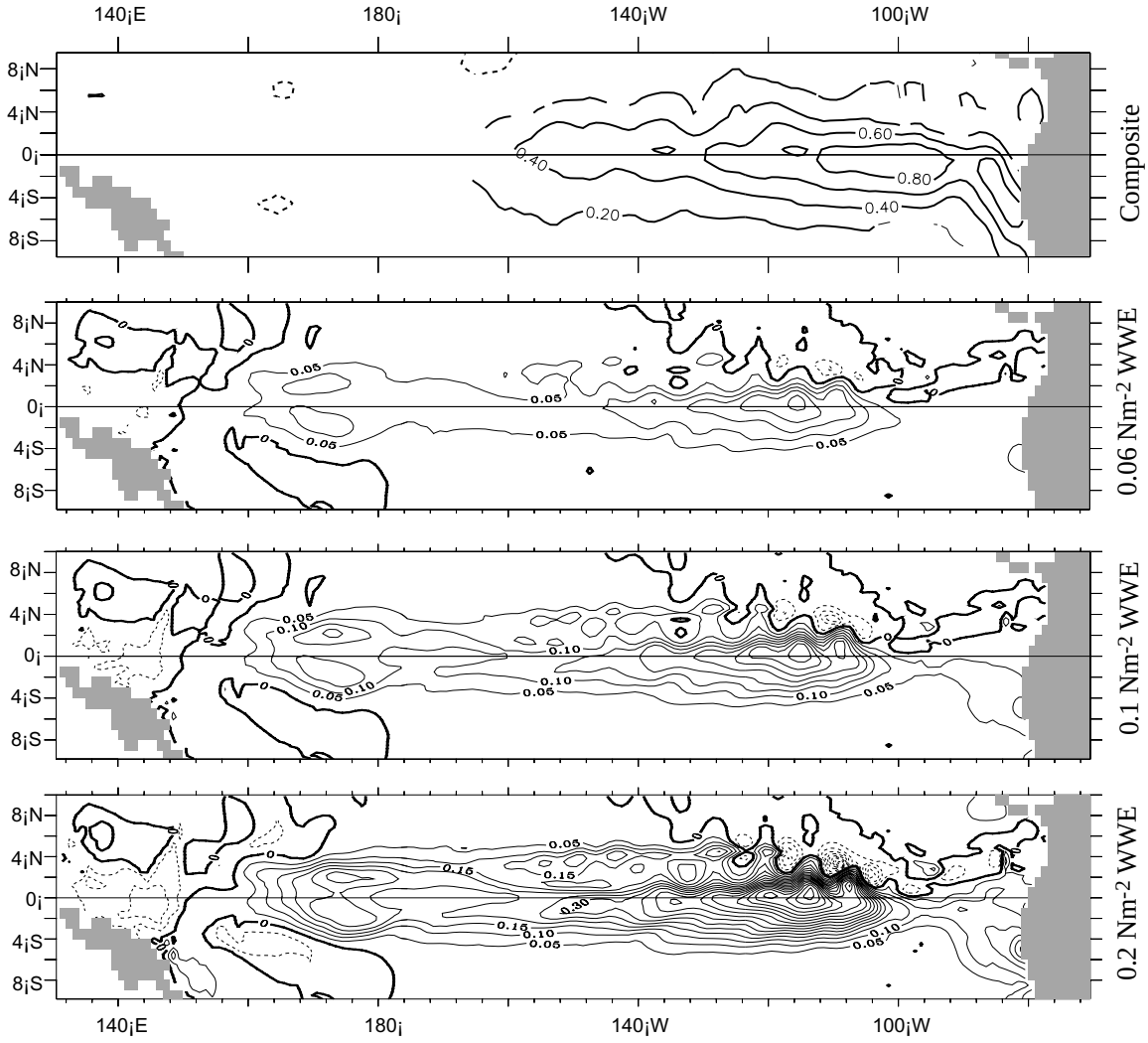

Figure V.10: SSTA Change 60 days after a Type C WWE from: (a) the 95% signficant ΔSSTA composite (contour interval 0.2°C), (b) Experiment C1 (countour interval 0.05°C), (c) Experiment C2 (contour interval 0.05°C), and (d) Experiment C3 (contour interval 0.05°C). Notice that the composite structure and the model structure are qualitatively similar in the region 165°W-100°W, where the initial conditions have a realistic zonal SST gradient.

eastern Pacific is increased to levels comparable to that near 110°W. The model reproduces the characteristics of the composite warming, within the limits of the model initial conditions.

A process which the model lacks, and could help explain some of the differences from observations, is coupling between the WWE driven SSTA response and the eastern and central Pacific surface stress fields and responsive clouds. ENSO is a coupled phenomenon characterized be wind and temperature changes across the basin (Rasmusson and Car-

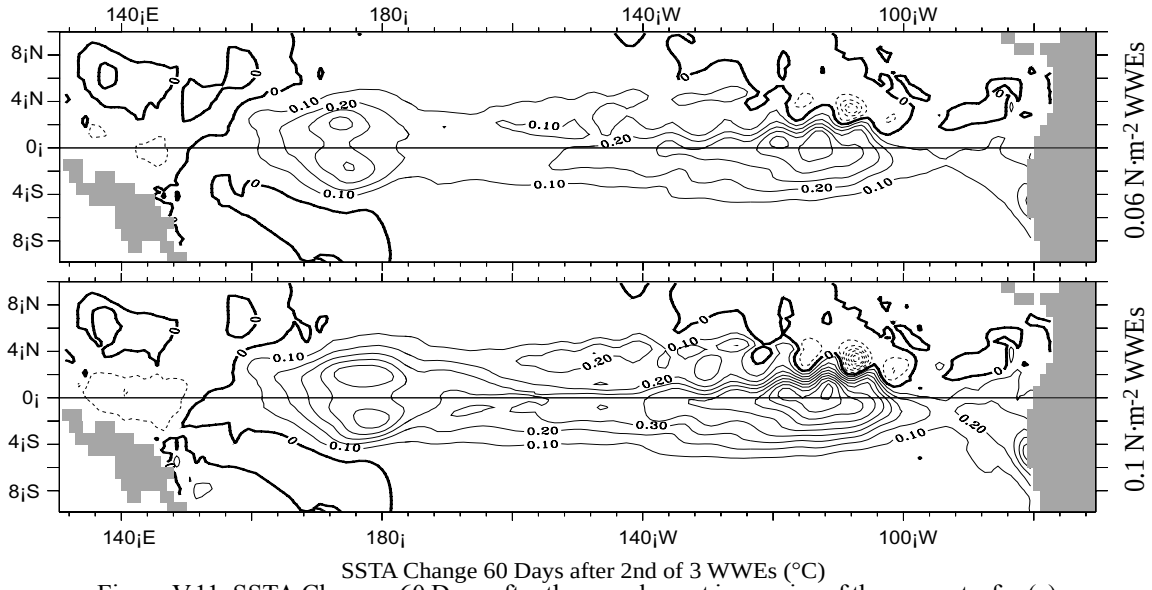

Figure V.11: SSTA Changes 60 Days after the seond event in a series of three events, for (a) Experiment C4, and (b) Experiment C5. Contour interval is 0.1°C. Notice how the warming along the coast of South America is more prominent, and the amplitude of the changes has increased, relative the single-WWE experiments. (Figure V.9)

penter 1982, Harrison and Larkin 1996, 1998.a), as well as changes in incoming solar radiation due to changes in stratus clous (Klein and Hartmann 1993). These experiments, with their prescribed eastern Pacific winds and clouds, will be unable to capture any coupling. This coupling would tend to produce enhancement of the of the warming through reduction of the intensity of the easterly equatorial trade winds, and the upwelling and vertical mixing driven by them. Also reduced by warming of the eastern equatorial Pacific is the stratus cloud coverage (Klein and Hartmann 1993), which would tend to enhance warming by allowing more incoming solar radiation to reach the far eastern Pacific.

In Section IV.4, it was noted that WWEs often occurred less than 40 days apart. Experiments C4-7 examine the effect of sequencing WWEs. The result is increased warming following each WWE. Also, for each WWE after the first, the warming along the coast of South America is enhanced relative the single event results. Figure V.10 shows the SSTA changes 60 days after the second of three WWEs for Experiments C4 and C5.

Sequencing the WWEs increases the anomalies changes after each WWE, and changes the structure of the anomalies after the second and third events to resemble the

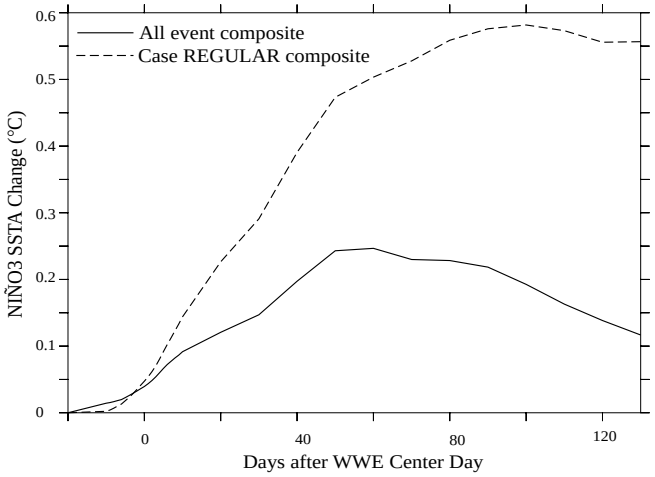

Figure V.12: Composite NIÑO3 SSTA Change (from Day (-20)) for the Type C all-event (solid line), and Case REGULAR (dashed line) composites. Units are °C.

composite more closely. Notice how the amplitude and structure of the east-of-dateline SSTA 60 days after the second and third events (Figure V.11.a-.b) is qualitatively similar to that of the composite (Figure V.10.a). The composite is still more diffuse in the meridional, a feature due to the smudging effects of averaging. The west of dateline anomalies are still stronger than expected from the composite; this additional warming is due to the incorrect SST gradient in the model. A sequence of three average amplitude WWEs (Experiment C4, Figure V.11.a) produces central Pacific equatorial warming of about a third the amplitude as that in the composite (Figure V.10.c); three stronger than average WWEs (Experiment C5, Figure V.11.b) produce central Pacific SSTA changes on the order of the composite.

A quantity of interest in the study of El Niño is the NIÑO3 SSTA index (SSTA averaged over the region 150°W-90°W, 5°S-5°N), and Type C WWEs are associated with warming of the NIÑO3 index (see Section III.4). Figure V.12 shows the Type C WWE composite change of the NIÑO3 SSTA index (from Day(-20)) for all events (solid line) and for Case REGULAR events (see Chapter III, dashed line). In both composites the index warms quickly following the WWE center day, reaching its maximum value somewhere between Day(40) and Day(60) for the all-event composite, and between Day(80) and Day(100) for the Case REGULAR composite. In the Case REGULAR composite the warm-

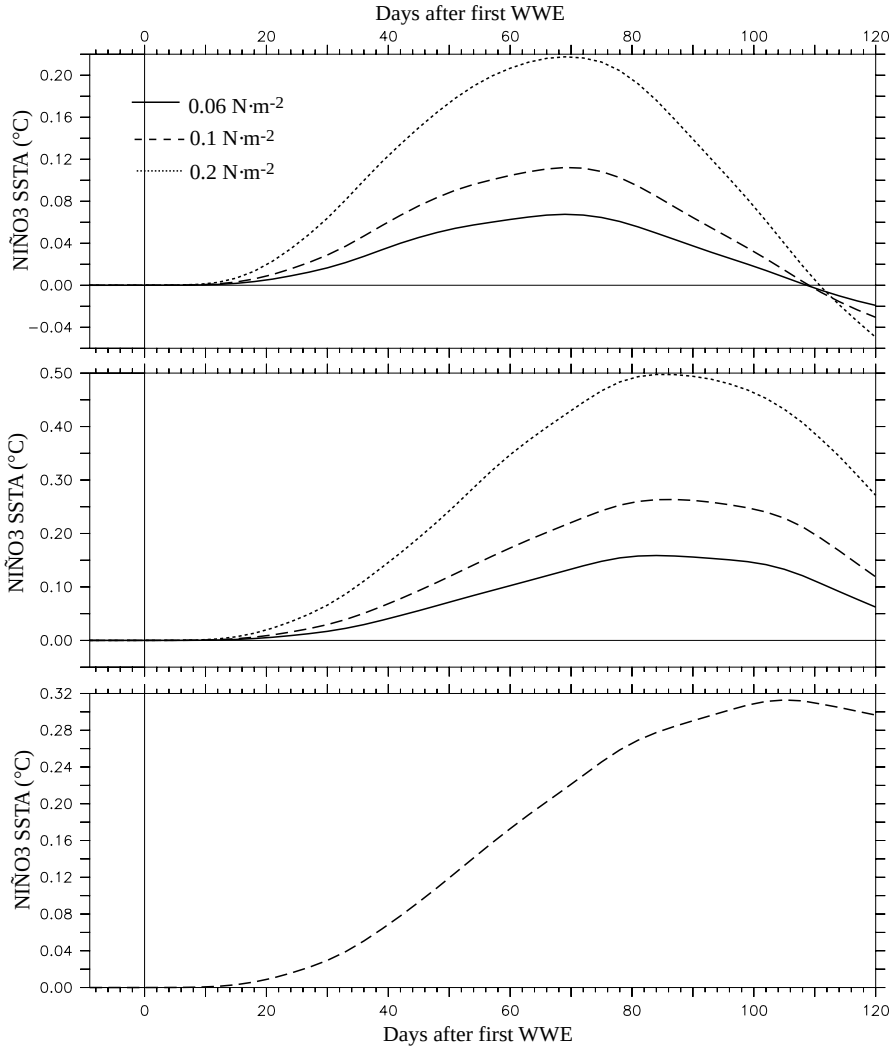

Figure V.13: NIÑO3 SSTA Change following (a) the single WWE experiments (C1-3), (b) the first event of the three WWE experiments (C4-6), and (c) the first event of the ten WWE experiment. In panels (a) and (b) the solid lines denote the 0.06 N·m^{-2} experiments, the dashed line denotes the 0.1 N·m^{-2} experiments, and the dotted line denotes the 0.2 N·m^{-2} experiments. Units are °C.

ing remains through Day(125).

Figure V.13 shows the NIÑO3 SSTA Index evolution for the single WWE cases (Experiments C1-3; upper panel), the three WWE cases (Experiments C4-6; middle panel), and for the ten WWE case (Experiment C7; lower panel). Notice how the amplitude of the NIÑO3 SSTA changes following the single WWEs (Figure V.13.a) appears to be relatively proportional to the WWE amplitude, with a 0.11°C maximum warming following the 0.1 N·m^{-2} burst and a 0.22°C maximum warming following the 0.2 N·m^{-2} burst. In the single

burst experiments, the timing of the maximum more closely resembles that of the all-event composite, occurring near Day(70); the warming disappears by Day(100). In the Experiments C1 and C2, the warming is fastest between Day(20) and Day (40) and slows, until the maximum is reached. In Experiment C3, a larger proportion of the warming happens before Day(40) than in the two weaker experiments.

For the three event experiments (Figure V.13.b), the amplitude of the maximum is increased, occurs later and lasts longer than for the single event experiments. The amplitude of the warming still appears to be somewhat linear, with a 0.25°C warming following the 0.1 $N \cdot m^{-2}$ bursts and a 0.5°C maximum warming following the 0.2 $N \cdot m^{-2}$ bursts. The effect of multiple WWEs is to raise and maintain NIÑO3 SSTA. The maximum in the three WWE experiments (Figure V.13.b), occurs near Day (90) and in the continued WWE experiment, the maximum occurs near Day(100). The continued WWEs in Experiment C7 maintain the NIÑO3 SSTA anomaly through Day(120), similar to the Case REGULAR composite.

In Chapter IV it was shown that the expected NIÑO3 SSTA changes following equatorial WWEs were independent to their association to the MJO (see Figure IV.21), and that the NIÑO3 SSTA changes following an MJO with an associated equatorial WWE were towards warming (see Figure IV.20). Experiment CM examines the SSTA changes following an MJO with a Type C event superimposed on it, in an attempt to reproduce the statistical relationships. Figure V.14 shows the equatorial SSTA in experiment CM. Notice how, as opposed to the MJO experiments (Exps. M1-4), the central and eastern equatorial Pacific warm following the termination of the MJO. The structure of the SSTA changes is similar to that following the Type C WWE (see Figure V.15,V.16). The character of the response is dominated by the WWE part, since the surface stress anomalies associated with the WWE are impulsive and much larger than those associated with the MJO. The model comfirms that the SSTA changes following an MJO with an equatorial WWE are similar to those following an equatorial WWE.

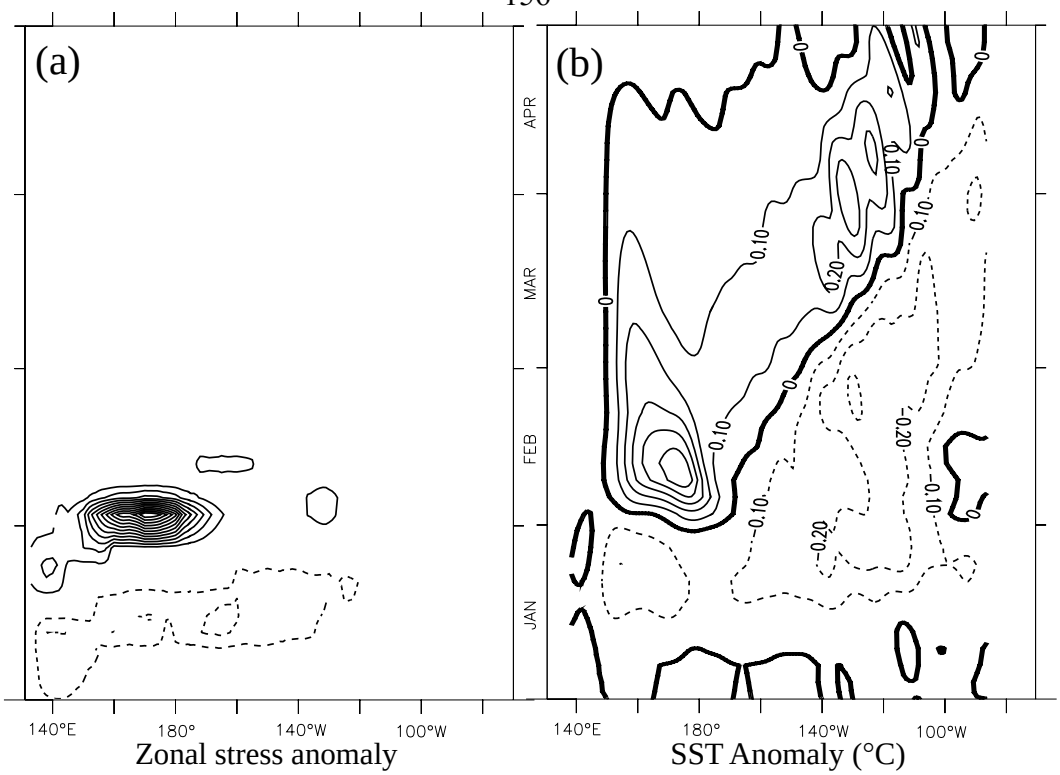

Figure V.14: Equatorial (a) Zonal stress anomaly ($N \cdot m^{-2}$), and (b) SST anomaly (°C), for Experiment CM. Contour interval in (a) is $0.5 \infty 10^{-2}$ $N \cdot m^{-2}$, contour interval in (b) is 0.1°C. Notice how the central equatorial Pacific warms following the WWE embedded in the MJO.

b. Mechanisms for SST Change:

In this section I examine the mechanisms which led to the WWE-driven equatorial SST changes in the OGCM. From Experiment C2, figure V.15 shows the time-longitude evolution of the 3-day-sampled equatorial: (a) Sea level height anomaly field, (b) SST anomaly field, (c) the thermocline depth field, and (d) the surface current anomaly field. The background shading indicates the expected 1st baroclinic and 2nd baroclinic Kelvin mode envelopes forced by the WWE; darker shading indicates the overlap between the two envelopes. Notice how the deepening of the thermocline, the raising of sea level height and the initial surface eastward acceleration coincide with the passage of the 1st baroclinic Kelvin pulse. Coincident with the 2nd baroclinic mode is a modification of the TIW field, and the largest amplitude SST anomalies. The modification of the TIW field leads to large amplitude meridional velocity anomalies, which overwhelm the WWE-forced signal, and pro-

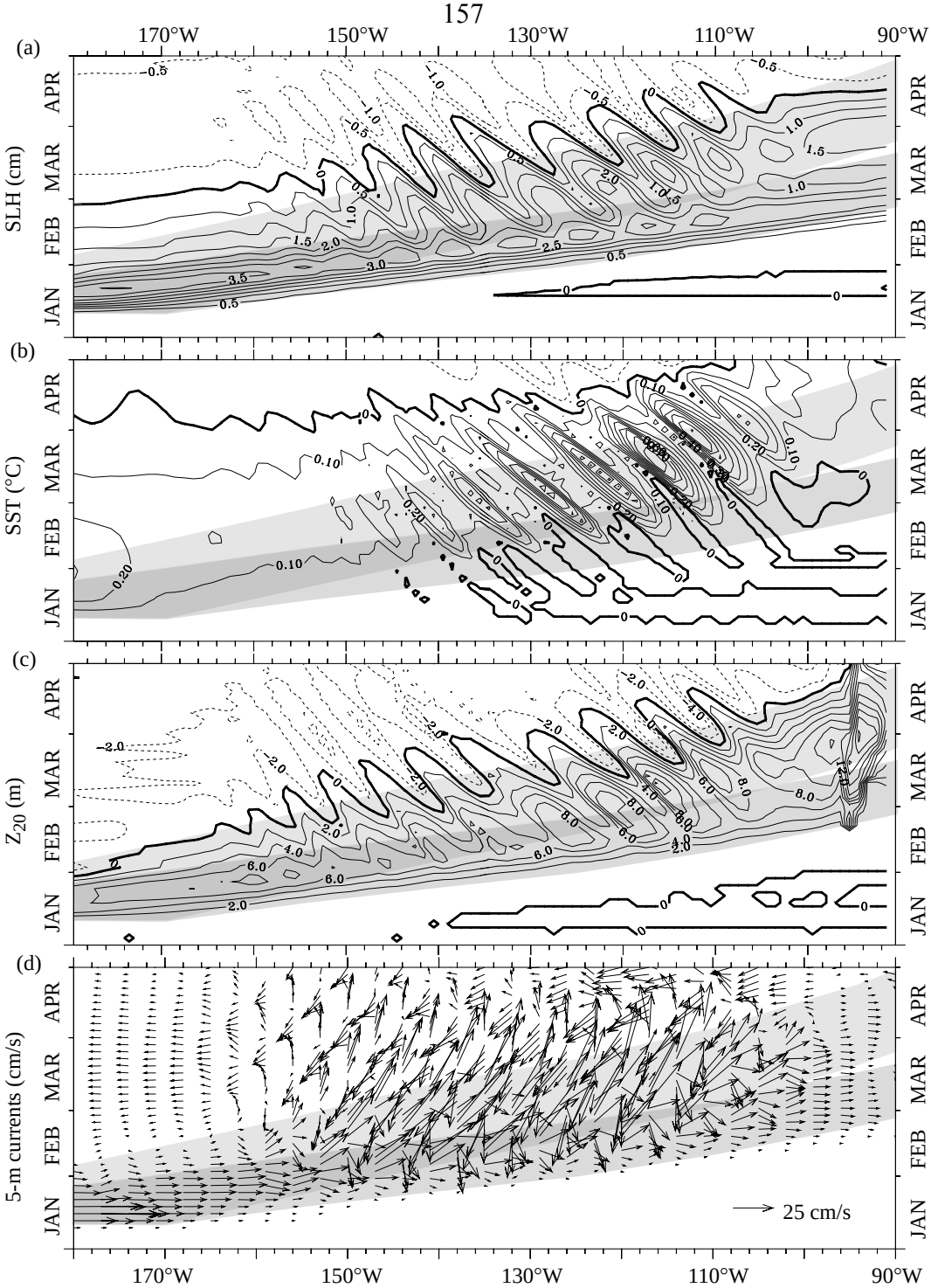

Figure V.15: East-of-dateline evolution of the 3-day sampled WWE driven anomalies along the equator, from experiment C2. (a) Sea level height anomalies in centimeters, (b) 5-meter temperature anomalies in °C, (c) thermocline depth (depth of 20°C isotherm) anomalies in meters, and (d) 5-meter current anomalies in cm/s. Shading in the background indicates first and second baroclinic mode envelopes, darker shading indicates the overlap between the two envelopes.

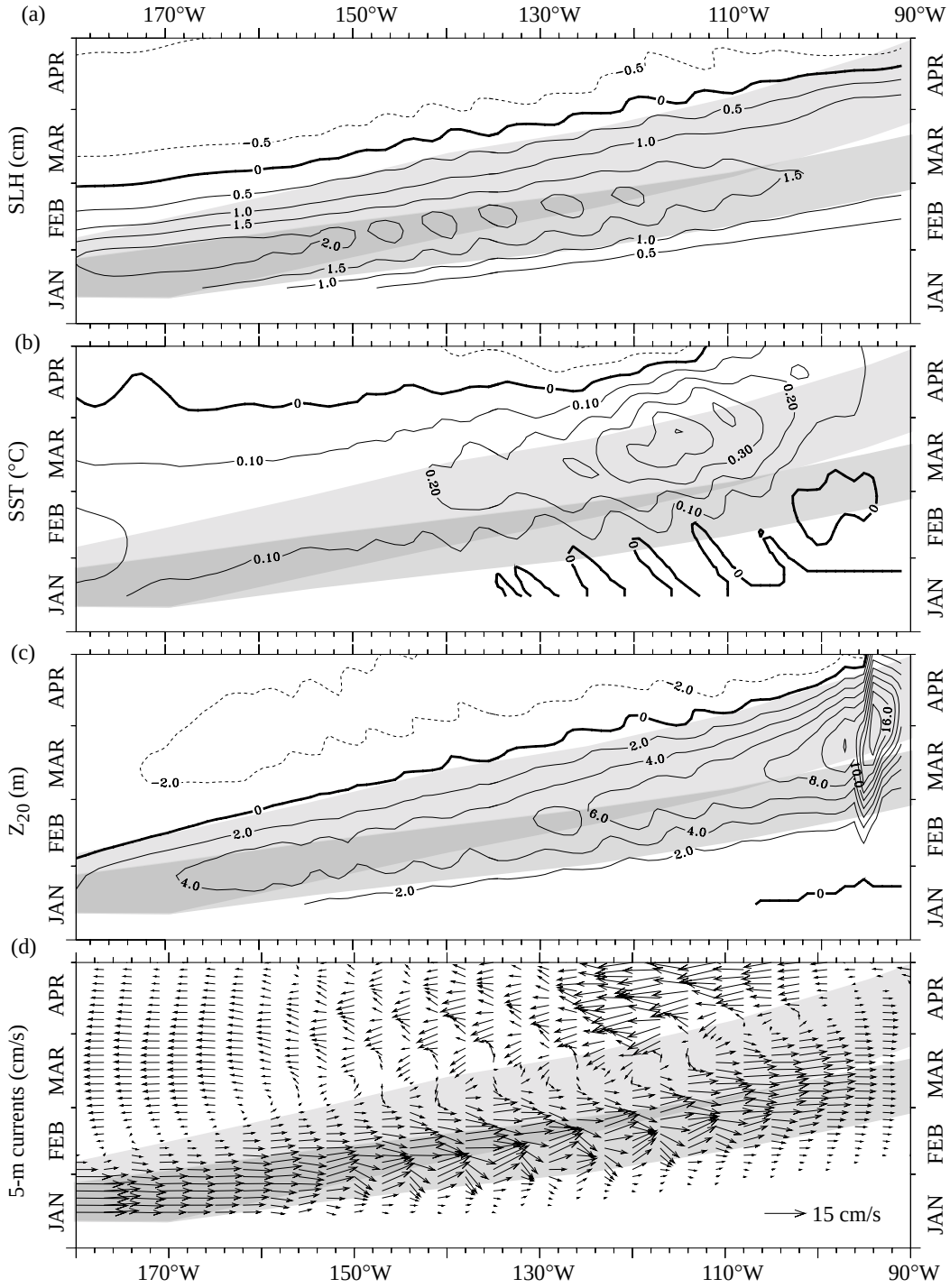

Figure V.16: East-of-dateline evolution of the 30-day boxcar smoothed WWE driven anomalies along the equator, from experiment C2. (a) Sea level height anomalies in centimeters, (b) 5-meter temperature anomalies in °C, (c) thermocline depth (depth of 20°C isotherm) anomalies in meters, and (d) 5-meter current anomalies in cm/s. Shading in the background indicates first and second baroclinic mode envelopes, darker shading indicates the overlap between the two envelopes.

duce large amplitude anomalies in all the plotted quantities.

To understand the evolution following the WWE it more useful to examine the 30-day boxcar smoothed evolution of the same anomalies.; these are shown in Figure V.16. Notice how the sea level height and thermocline depth anomalies appear with the 1st baroclinic mode, and return to zero as the 2nd mode passes. The surface current anomaly field is largely zonal, with eastward acceleration following the 1st baroclinic mode, but continuing into the 2nd. The maximum eastward currents correspond to the overlap between the 1st and 2nd mode envelopes, and in the far eastern Pacific where the two modes separate there appear to be two zonal current maxima. In the central Pacific sea level rising, thermocline deepening, zonal acceleration and SST warming reach a maximum at the overlap between the 1st and 2nd mode. While the 1st baroclinic mode propagates at ~2.8 ms^{-1} and the 2nd mode propagates at ~1.8 ms^{-1}, the maximum anomalies propagate at ~2.4 ms^{-1}. This propagation speed is the speed of the overlap between the two baroclinic modes.

The relative timing of the various quantities in the surface layer are more clearly seen in timeseries across the basin. Figure V.17 shows timeseries of the evolution of the uppermost layer of the model in Experiment C1-3. Each column is a separate location along the equator, from 155°W to 95°W (corresponding to the location of the TAO buoys). The rows show the 30-day boxcar smoothed evolution of anomalies in SST, thermocline depth, surface zonal current, surface meridional current, and 20-m vertical velocity. As in Figures V.15 and V.16, the envelopes of the 1st and 2nd baroclinic Kelvin pulses are shown by the background shading, with the dark shading indicating the overlap between the two modes. The solid line is for experiment C1, the dashed line is for experiment C2, and the dotted line is for experiment C3.

Notice, in Figure V.17, that the initial thermocline deepening and zonal current acceleration is coincident with the arrival of the 1st baroclinic mode, while the main surface warming generally occurs with both the 1st and 2nd baroclinic mode. The surface current is

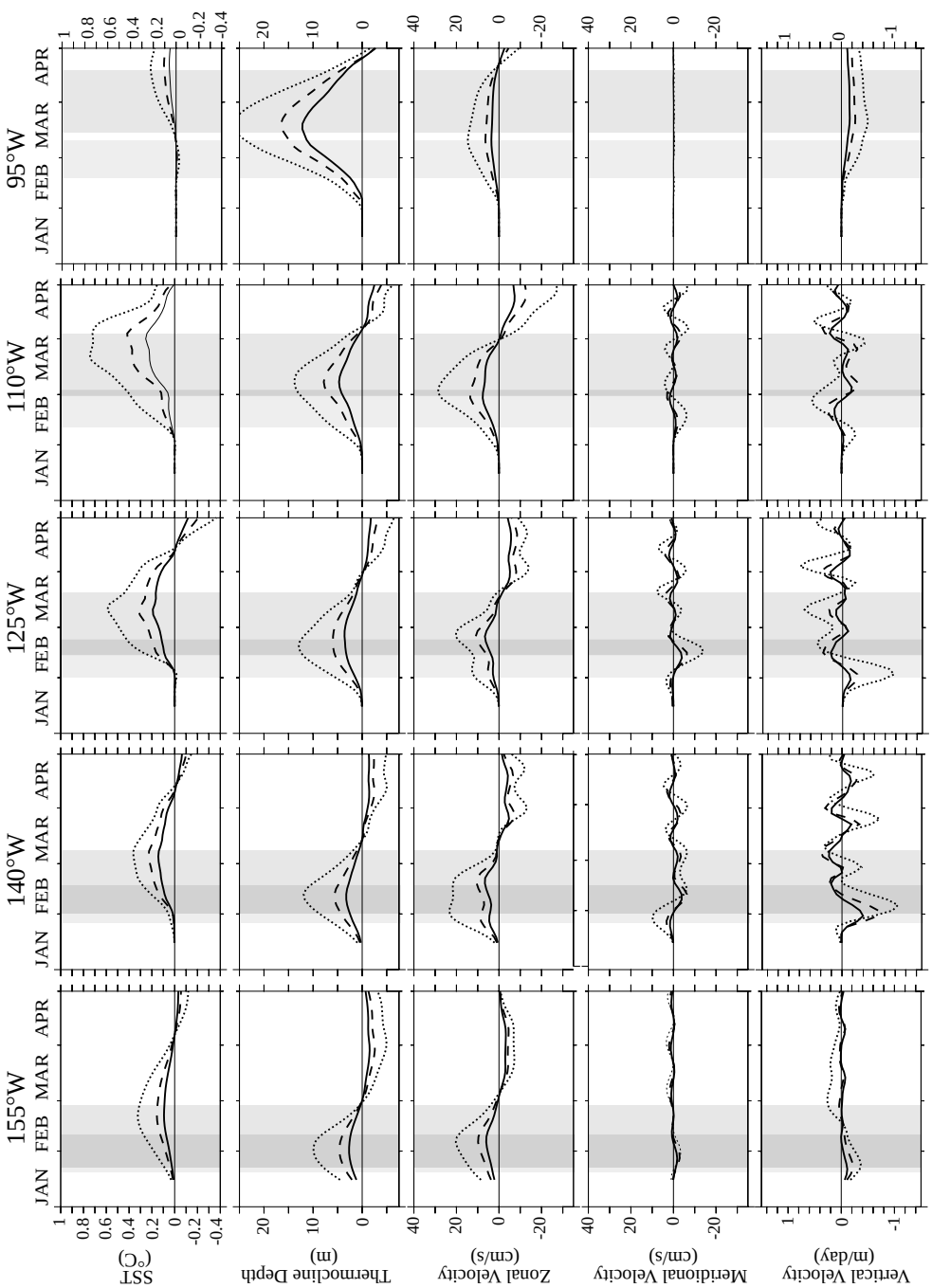

Figure V.17: Timeseries of the 30-day boxcar smoothed evolution of the the model for experiments C1-3 across the equator from 155°W to 95°W. Starting at the top row: 5-meter temperature anomalies, Thermocline depth anomalies, 5-meter zonal current anomalies, 5-meter meridional velocity anomalies, and 20-meter vertical velocity anomalies. Solid line is for experiment C1, dashed line for experiment C2, and dotted line for experiment C3.

accelerated eastward and thermocline is deepened by the first and second baroclinic mode passes,with the maximum anomalies in the overlap of the first two modes. Notice how even with the 30-day boxcar smoother, between 140°W and 110°W the main meridional and vertical velocity anomalies have a period similar to the TIWs, and result due to differences in the TIW fields. It would be difficult to measure differences such as these, because they result from differences between two instability wave fields. At 95°W the vertical velocity field is dominated by downwelling begining with the arrival of the 1st baroclinic mode and continuing with the 2nd baroclinic mode.

Timeseries of the 30-day boxcar smoothed anomalous balance of terms for temperature averaged over the top 20 meters across the equator is shown in Figure V.17, for Experiments C1-C3. The first column shows the temperature tendency term (ðT/ðt), the second column shows the negative advection of temperature, and the third column shows the diffusive including the surface heat flux anomaly. Notice how the warming is generally related to anomalous temperature advection, and after there has been some warming, there begins to be diffusive and heat-flux anomalies. The diffusive anomalies in most locations (except in February at 140°W and 125°W) are dominated by the tendency of the surface heat-flux to oppose the anomalous warming, thus the term appears as a cooling term.

Figure V.19 parses the advective term into its components, at each location I show: the total negative advection anomaly, the negative zonal advection anomaly, the negative meridional advection anomaly and the negative vertical advection anomaly. The intial dominant advective term in the heat balance varies with location: zonal advection dominates in the central basin (155°W and 140°W), vertical advection dominate in the eastern basin (125°W and 110°W), and in the far west warming due to vertical advection is opposed by cooling due to zonal advection (95°W). Between 155°W and 110°W meridional advection is an important term following the initial warming; this is a region with TIW activity in the model. There is warming due to meridional advection at 155°W and 110°W,cooling due to

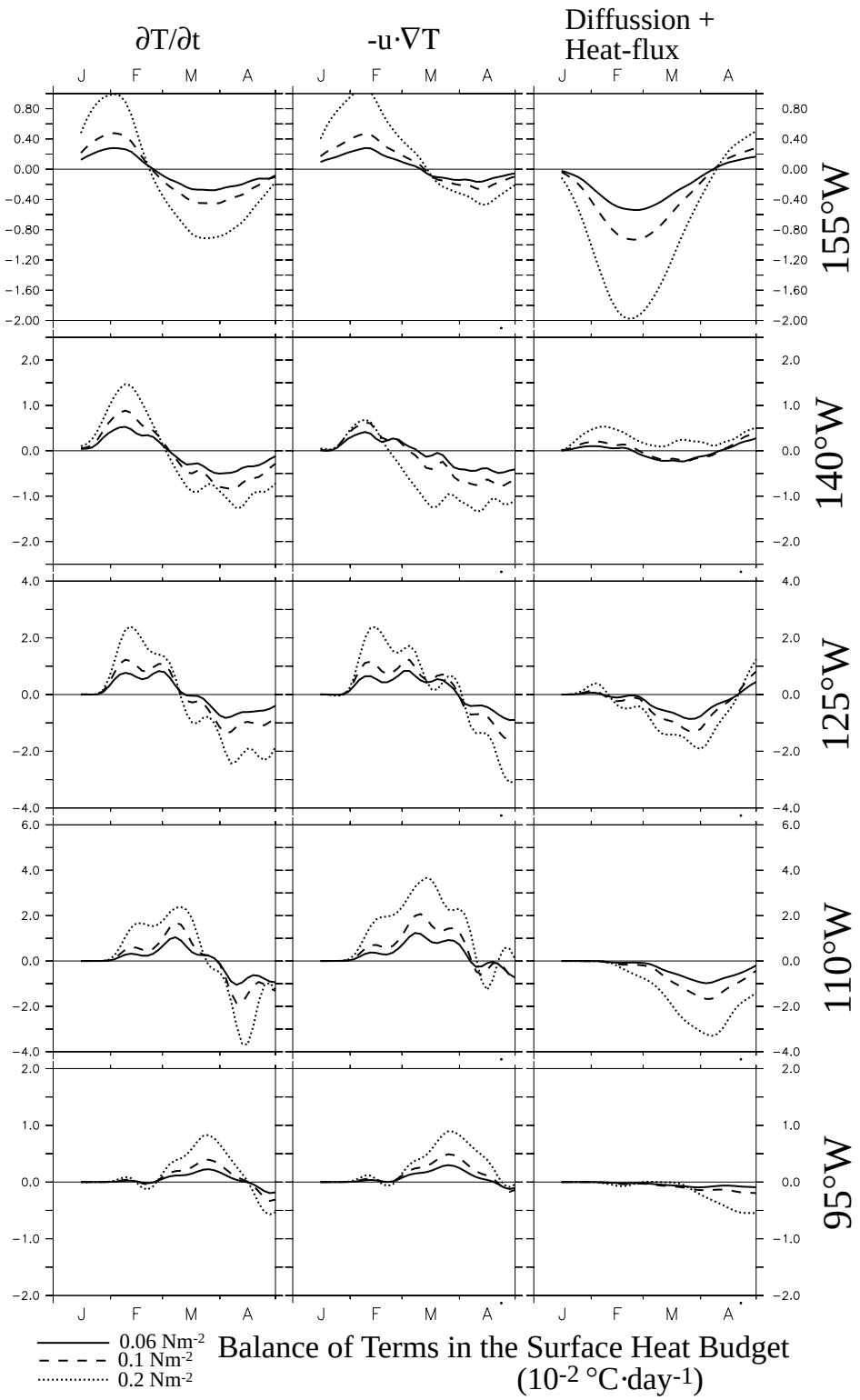

Figure V.18: Heat balance of the upper 20 meters for Experiments C1-3 along the Equator from 155°W through 95°W. Units are 0.1°C/day. Notice that the vertical axes are different for each longitude.

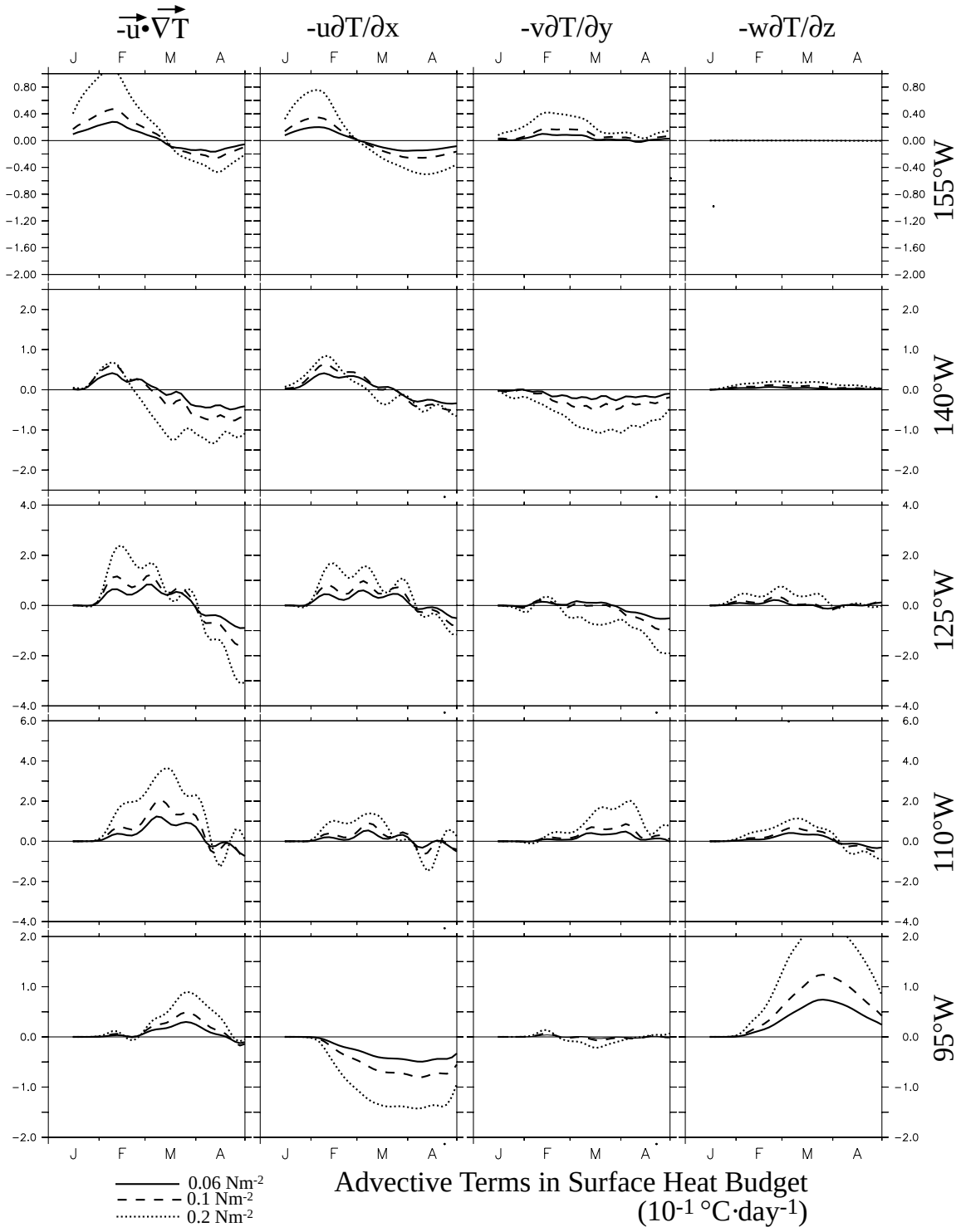

Figure V.19: Breakdown of the advective terms in the hear balance of the upper 20meters for Experiments C1-3 along the Equator from 155°W through 95°W. Solid line is for experiment C1, dashed line for experiment C2, and dotted line for experiment C3. Units are 0.1°C/day. Notice that the vertical axes are different for each longitude.

anomalous meridinal advection at 140°W and 125°W.

Anomalous advection of temperature has three components: advection of the background temperature gradient by the anomalous currents (**u'· T**), advection of the anomalous temperature gradient by the background currents (**u· T'**), and advection of the anomalous temperature gradient by the anomalous currents (**u'· T'**). At none of the locations is the third term (**u'· T'**) dominant to the anomalous SST. In most locations the main SST warming is initiated by advection by anomalous currents (**u'· T**); a notable exception is 95°W where vertical advection of the anomalous temperature gradient leads to the main surface warming. In the central Pacific, the SST warming is dominated by (**u'· T**), since the termocline is generally deeper than the background meridional upwelling cell (~50 m). In the eastern Pacific, since the thermocline is often shallower than the meridional upwelling cell,vertical advection of anomalously warm water becomes an important term (a dominant one at 95°W). Except in the far eastern Pacific, thermocline deepening occurs prior the SST warming forced by WWEs (see Figure V.15-V.17), however this thermocline deepening is not driving the warming. Rather, the surface warming is being driven by anomalous currents, whose convergence causes the thermocline to deepen.

5. Summary and Conclusions:

I have attempted to reproduce the SSTA changes statistically associated with the MJO and WWEs in the eastern and central Pacific using an OGCM. I also examined the mechanisms responsible for those changes. The composite MJO zonal stress anomalies do not drive eastern Pacific waveguide warming during the lifetime of the event. Equatorial WWEs drive circulation changes which result in eastern and central equatorial Pacific SST warming resembling that observed in the SSTA composites (see Chapter III). WWEs provide a mechanism for the onset of El Niño SSTA, through advection of the backgroud SST gradient.

MJO-driven surface wind variability over the western and central Pacific has been suggested as an important mechanism for waveguide SST warming during El Niño (Lau and Chan 1986, 1988, Lau and Shen 1988, Weickman 1991, Kessler *et al.* 1995, Moore and Kleeman 1999). The surface wind structure of the MJO has been idealized as a sinusoid confined to the western Pacific warm pool (Kessler *et al.* 1995, Kessler and Kleeman 2000). These idealizations are inconsistent with the composite surface wind structure of the MJO using the Maloney and Hartmann (1998) MJO index (see Chapter IV), and with the MJO-related equatorial surface zonal stress described by Hendon *et al.* (1998).

The absence of correlation between El Niño waveguide warming and enhanced MJO activity is consistent with the results of forcing the OGCM with composite MJO surface wind stress. There is no correlation between enhanced MJO activity and El Niño waveguide warming (Slingo *et al.* 1999, Hendon *et al.* 1999, Harrison and Vecchi 2000, Figure IV.2). Certain MJO events, which co-occur with equatorial WWEs, tend to be followed by equatorial waveguide warming (see Figure IV.19), yet this warming is not significantly different from that which follows equatorial WWEs which occur without the MJO. The warming is a feature of the WWEs, not of the MJO.

A significant feature of the surface wind and wind-stress field associated with the MJO is periods of easterly and westerly flow across most of the equatorial Pacific (Figure V.2-.3). When the model is forced with the statistically significant MJO zonal stress anomalies, the eastern and central equatorial Pacific SST cools. The central Pacific cooling is driven by the central Pacific easterlies which dominate the composite, while the eastern Pacific cooling is forced by both the central Pacific and western Pacific wind stress anomalies (Section V.3). A sequence of MJOs produces cooling in excess of 0.3°C across most of the eastern and central equatorial Pacific, during and in the month following the MJOs (Figure V.11). When the mean over the period of an MJO is removed from the zonal stress anomaly field, the effect of the MJO on the model is to produce very small cooling during

the forcing period. The composite MJO zonal stress field is not suggestive of the MJO driving eastern and central Pacific waveguide warming during the onset of El Niño. These experiments lack coupling of the ocean and atmosphere, which has been suggested as an important mechanism for the evolution of the SSTA field following the MJO (Kessler *et al.* 1995, Kessler and Kleeman 2000), their results idicate that there is a coupling between the MJO driven SSTA changes and the location of the maximum westerlies in the surccessive MJO events. It would be of interest to repeat the coupled experiments of Kessler *et al.* (1995) and Kessler and Kleeman (2000) with the MJO forcing derived using the MH98 MJO index, which exhibits zonal stress anomalies far beyond the eastern edge of the warm pool.

Prior to the return of SST to normal at the end of recent El Niño events, there has been a shoaling of the eastern equatorial Pacific thermocline to normal or shallower than normal depths; this thermocline shoaling makes cool water available to be upwelled by equatorial easterly winds (Harrison *et al.* 1990, Kessler and McPhaden 1995, Harrison and Vecchi 1999, 2000, McPhaden 1999, McPhaden and Yu 1999). This thermocline shoaling might be due to "delayed-oscillator" type mechanisms (see Suarez and Schopf 1988, Battisti and Hirst 1989, Neelin *et al.* 1998), or to the interaction of the seasonal cycle with anomalous El Niño conditions (Harrison and Vecchi 1999), or a combined effect of the two. During weak or moderate El Niño events, such as 1986-7 or 1991-2, when easterly trade winds remain present to some degree through the event, the shoaling thermocline makes cool subsurface water available to the shallow upwelling circulation and returns eastern Pacific SST towards climatology. In extreme El Niño events – such as 1982-3 or 1997-8 – during which the easterly trade winds weaken and even disappear across the Pacific, the cool subsurface waters, brought close to the surface by the thermocline shoaling, do not break through to the surface until equatorial easterlies return. The presence of equatorial easterlies in the MJO-composite, when NIÑO3 SST is warmer than normal (see Section IV.3.a), suggests

the MJO as a potential mechanism for eastern Pacific SST cooling at the end of major El Niño events.

Takayabu *et al.* (1999) have suggested that the abrupt termination of the 1997-8 El Niño event was related to central equatorial Pacific easterly winds associated with an MJO in May 1998. Figure IV.2 shows that MJO events passed across the tropical Pacific in June 1983 and May 1998, coincident with the rapid cooling to normal SST at the end of these to major El Niño events (during which the easterly trade winds became extremely weak and even disappeared; see Harrison *et al.* 1990, McPhaden 1999, McPhaden and Yu 1999). As the thermocline shoaled at the end of these major El Niño events, horizontal surface temperature gradients were weak and there was little evidence for equatorial upwelling. Once the thermocline shoaled, a large vertical temperature gradient was set up in the central/ eastern equatorial Pacific; and since the entire equatorial Pacific had SST in excess of 28°C the MJO-related stresses over the entire Pacific should be in the convective regime. The convective regime is characterized by a quasi-oscillatory propagating zonal stress variability (see Figures 4,5,7). Westerly stress anomalies over the equatorial Pacific tend to lead to warming, primarily through advective processes; in the absence of horizontal gradients and background upwelling one would expect the effects to be small. Easterly stress anomalies over the equatorial Pacific tend to drive surface cooling through advective, heat-flux and mixing processes; since the vertical temperature gradient is the dominant temperature gradient across the equatorial Pacific, one would expect the effect of the easterly Phases of the MJO to be cooling of the eastern and central equatorial Pacific. Thus, the MJO provides a mechanism for the return of SSTA to normal when the background easterly trades are weak.

Equatorial WWEs have been suggested as a mechanism for the onset of El Niño waveguide warm anomalies. WWEs are observed to precede El Niño (Keen 1982, Luther *et al.* 1983, Harrison and Giese 1989,1990, Harrison and Vecchi 1997) and are linked with the onset and maintenance of warm conditions (Vecchi and Harrison 2000, Chapter III). Ocean

general circulation model (OGCM) experiments have suggested that equatorial WWEs can drive El Niño eastern and central equatorial Pacific SST changes (Harrison and Giese 1988, Giese and Harrison 1990,1991, Kindle and Phoebus 1995). WWEs with realistic (x,y,t) scales drive SSTA changes consistent with the observed associations (Chapter III).

The central equatorial Pacific SSTA driven by individual WWEs is similar to that in the associations, however the amplitude for average amplitude WWEs is much smaller than the associated changes. However, when WWEs are placed in succession, they reproduce the amplitude and the structure of the composite SSTA changes. Since WWEs often occur within 40 days of each other (see Figures IV.15-.16), the composites represent the effect of more than one WWE. The OGCM is unable to reproduce any ocean/atmosphere coupling in the eastern and central Pacific; this coupling would strengthen the warming response of the system.

Following the WWE, theermocline deepens, sea level height rises, surface zonal current accelerates and SST warms in association with both the first and the second baroclinic modes. The maxima in zonal current, thermocline depth and sea level height anomaly occurs at the overlap between the first and second baroclinic wave envelopes. The maximum propagates eastward at the speed of the overlap of the first and second mode (~2.4ms^{-1}), which does not correspond to the speed of the first or second mode envelopes (~2.8ms^{-1}, and ~1.8ms^{-1}, respectively). In the far eastern Pacific (95°W), there is almost no SST signal until the expected arrival of the second baroclinic mode. However, most of the warming in the far eastern Pacific is not driven directly by the pulse, but rather results from thermocline deepening associated with the current pulse.

The warming following the WWE is initially driven by SST advection, after which vertical mixing and anomalous heat flux become important terms. There are three regimes in the eastern and eastern-central Pacific, based on which advective term which initiates the warming. In the central Pacific (155°W and 140°W) zonal advection by the WWE driven

pulses drive the initial warming. Near 125°W and 110°W zonal and vertical advection are important for the initial warming. In the far eastern Pacific (~95°W) warming is dominated by vertical advection, and opposed by zonal advection of the background positive *ðSST/ðx;* the warming is associated both with advection of the background temperature gradient by the anomalous vertical currents and advection of the anomalous temperature gradient by the background upwelling circulation. Between 155°W and 110°W meridional advection is a significant term following the initial warming, this is a region of strong TIW activity.

The results for the WWE experiments using realistic zonal scales are consistent with those of Harrison and Giese (1988) and Giese and Harrison (1990, 1991). The character of the SSTA changes following WWEs with a zonal length scale of ~30° and with a zonal length scale of ~20° is similar. Both suggest that WWEs drive eastern and central Pacific SST warming similar to that seen during El Niño.

Equatorial WWEs, with duration typically in the 6-20 day range, have been strongly associated with equatorial SSTA warming (if the initial state of the ocean was normal or cooler than normal) and with the maintenance of warm SSTA (if the ocean was already significantly warmer than normal). OGCM experiments have established mechanisms by which WWEs cause SSTA to increase or maintain warm SSTA. WWEs are a fundamental mechanism in El Niño waveguide SST warming and warm anomaly maintenance. The surface wind anomaly field associated with the MJO is dominated by eastern and central Pacific easterlies, providing a potential mechanism for the return to normal SST at the end of extreme El Niño events and for cooling during La Niña events. Equatorial SSTA changes following an MJO with a superimposed equatorial WWE are of similar character to those following an equatorial WWE (Figure V.13). The surface stress anomaly associated with an average WWE (0.06 $N \cdot m^{-2}$) overwhelms the surface stress anomaly associated with the average MJO (0.01 $N \cdot m^{-2}$).

The importance of sub-seasonal atmospheric variability in ENSO is apparent: WWEs

are a fundamental mechanism for the onset and maintenance of El Niño warming, and the MJO may be important in the termination of certain extreme El Niño events. Because there is so much energy in the sub-seasonal band, and because westerly wind events have been strongly connected with the onset and maintenance of El Niño, further study of the sub-seasonal band is important for understanding the life-cycle of El Niño. In particular, improvement in our ability to predict the onset and amplitude of El Niño warming is likely to come from improved understanding of the entire sub-seasonal band of tropical Pacific wind variability. Improved forecasts of the onset, amplitude and termination of El Niño events will likely depend on improved understanding and prediction of WWEs, the MJO, cyclones, cold surges and convective superclusters, and their interconnections.